Approximating the energy landscape of a two-dimensional bistable gene autoregulation model by separating slow and fast dynamics

Xu Dong Wang, Yin Jie He, Jun Tang,[*] and Long Bai
School of Physics, China University of Mining and Technology, Xuzhou 221116, China

Jun Ma
Department of Physics, Lanzhou University of Technology, Lanzhou 730050, China

The energy landscape is widely used to quantify the stability of multistable nonlinear systems, such as bistable gene regulation networks. In physics, the potential can be obtained through integration only for gradient systems. However, multidimensional nonlinear systems are often nongradient, for which the potential is calculated by decomposing the dynamics to gradient and nongradient parts. This potential is then called a quasipotential. Given that one-dimensional (1D) systems can be regarded as gradient systems, we attempt to separate the two-dimensional (2D) system into two 1D systems working on distinct timescales, and the potential can be easily calculated for the two 1D systems separately. This method is used in this study to estimate the energy landscape of a two-variable gene autoregulation model. This elegant and comprehensive method is accessible for 2D nonlinear systems in which the dynamics can be divided into slow and fast parts.

I. INTRODUCTION

On the basis of Waddington's epigenetic landscape, considerable efforts have been made to describe the stability of nonlinear dynamical systems, especially biological systems, through energy landscape [1,2]. In systems described by nonlinear differential equations, energy landscape indicates the graph of the potential function across the configuration space of the systems. The following nonlinear system is considered:

$$\frac{d\boldsymbol{x}}{dt} = \mathbf{F}(\boldsymbol{x}),$$

where vector $\boldsymbol{x}(t) = (x_1(t), x_2(t), \ldots, x_N(t))$ denotes the developing state of the system and N represents the number of dimensions. "Driving force" $\mathbf{F}(\boldsymbol{x})$ is often nonlinear for biological systems. In physics, the potential can be obtained through integration only for gradient systems. However, multidimensional nonlinear systems are generally nongradient. A prevalent scheme is to decompose the nongradient driving force $\mathbf{F}(\boldsymbol{x})$ to two components: gradient and nongradient parts. The decomposition should guarantee that the potential corresponding to the gradient part exactly presents the state-developing barriers of the systems, and the other part is not required for state changing. The potential integrated from the gradient component is defined as "quasipotential." As reviewed by Zhou *et al.* [2], several methods have been introduced to decompose the driving force. The so-called Helmholtz decomposition allows the three-dimensional (3D) vector field to be uniquely decomposed into the sum of the gradient field and divergence-free curl term. Zhou *et al.*

proposed a decomposition of vector fields that permits the computation of a quasipotential function that is equivalent to the Freidlin-Wentzell potential [2]. Ao *et al.* [3,4] constructed the quasipotentials through symmetric and antisymmetric decompositions. Numerous works have also attempted to decompose the driving force on the basis of probability flux, which is included in the master equations [5–10]. Zhou *et al.* discussed the mathematical details in Ref. [2].

Zhang *et al.* estimated the one-dimensional (1D) potential of a two-dimensional (2D) nonlinear system via quasi-steady-state approximation on the slow variable [11]. This approach is appropriate only for the systems in which variables evolve on dramatically different time scales. Although Zhang's method fails to calculate the potential for all state points in the multidimensional space, it enlightens us to divide the dynamics of the multidimensional system into different timescales, i.e., decompose the 2D system into two 1D systems working on distinct timescales. After all, one-dimensional systems can be regarded as gradient systems. This assumption may simplify the task of calculating the 2D potential to deal with two 1D potentials. This comprehensive assumption also prevents us from understanding the complicated mathematical conceptions about vector fields in the currently available decomposition methods.

Energy landscape has been used to quantify the stability of multistable nonlinear systems. Multistability is a widespread phenomenon in biological, physical, and chemical systems [12]. In biological systems, multistability is associated with numerous biological functions. Complex gene networks store memory by creating two or more discrete, stable states of network activity [13–15]. In *Escherichia coli*, multistability has been experimentally demonstrated to account for the maintenance of phenotypic differences in the absence of genetic or environmental distinctions [16]. Multistability has been

---
[*]Author to whom correspondence should be addressed: tjuns1979@126.com

invoked to explain the cell cycle regulatory circuits in *Xenopus* and *Saccharomyces cerevisiae* [17,18], and the generation of switchlike biochemical responses [19,20]. In nonlinear dynamics, multistability may originate from the interaction between multiple positive or negative feedback. For example, mutual regulation of multiple genes may produce multiple stable states with distinct concentrations of corresponding proteins [21,22].

In the gene regulation network, feedback loops act as building blocks for shaping cellular functions, such as oscillation, hysteresis, and bistability. NF-κB signaling pathway regulates a number of cellular processes including survival, inflammation, and immune response, in which the IκB family and IKK mediate a strong negative feedback regulation on NF-κB activation, resulting in the damped oscillation of the NF-κB activation profile [23,24]. A genetic toggle switch can transform a continuous morphogen gradient into distinct domains of gene expression [25–27]. This type of transcriptional mechanism exists in numerous biological subsystems, in which the expression of one set of factors represses the alternative identity, and vice versa, thereby creating a bistable switch [28,29]. A genetic toggle switch plays an essential role in the decision making of a cell and a discrete response to an external signal [5,30–32]. In general, one transcription factor (TF) regulates a number of genes including itself. This characteristic determines the connectivity of the gene regulation network. TFs in *E. coli* seldom regulate the transcription of other genes besides itself. Thus, we focus on the autoregulation network, in which the TF regulates the transcription of its encoded gene.

The energy landscape for gene regulation networks is usually used to exhibit the cell fate decision, transition between multistates. We attempt to implement our method of separating the timescales of a 2D system on a bistable gene autoregulation model. The energy landscape helps us understand the convergence dynamics of the gene expression to its stable states. The 2D dynamics of the gene autoregulation model is divided into two 1D dynamics (slow and fast parts) through similitude transformation, and the potentials are calculated on different timescales. Then, the 2D potential surface is obtained by integrating the two 1D potentials. In Sec. II, the gene autoregulation model is introduced. In Sec. III, the central manifold of the model is determined by dividing the dynamics of the system to slow and fast parts. The 1D potentials of the fast and slow dynamics are calculated. Then, the 2D energy landscape is estimated by integrating the 1D potentials. In Sec. IV, the conclusions are drawn.

II. MODEL

Following Ref. [33], we consider a gene autoregulation loop, which is schematized in Fig. 1. On the basis of one gene, successive transcription and translation processes lead the production of encoded protein, which, in turn, regulates the expression of that gene. The regulation can be repression or activation. To obtain a multistable behavior, we focus on the case of gene activation. Although diverse response of mRNA abundance to protein concentration has been reported in theoretical works [34,35], experimental results tend to support a Michaelis-Menten type [36]. The model equations
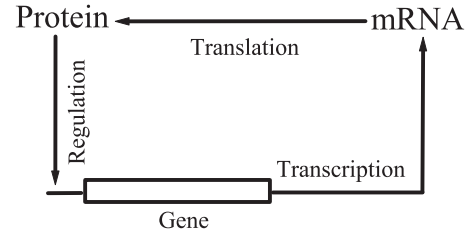

FIG. 1. Schematic of the gene autoregulation loop.

are as follows:

$$\dot{x} = \beta \frac{z^m}{\gamma + z^m} + \varphi - \delta x,$$
$$\dot{z} = \rho x - \tau z, \qquad (1)$$

where x and z represent the concentrations of mRNA and protein, respectively. Parameters δ and τ denote the effective decay constants of mRNA and protein, which may involve degeneration and dilution due to cell growth. φ is the basal transcription rate, and m refers to the Hill coefficient which often depends on the number of DNA binding sites. The constant parameter values are $\beta = 6$, $\rho = 0.5$, $\delta = 0.5$, $\tau = 0.1$, and $\varphi = 0.2$. On the basis of these parameter settings, Arani *et al.* reported that the system can be bistable only when the Hill coefficient $m > 1$. Thus, we will set $m = 2$ when no special statement exists. The system is bistable when $4.63 < \gamma < 10.28$, but monostable when $\gamma < 4.63$ or $\gamma > 10.28$.

All numerical integrations of the model are performed by using the fourth-order Runge-Kutta scheme with a time step of 10^{-3} time unit. Simulations further verify time step reduction does not considerably improve accuracy.

III. METHOD AND RESULTS

As previously mentioned, we attempt to calculate two 1D potentials on the basis of two separated timescales. The timescales of variables x and z are not separated enough, as shown in Figs. 2(a) and 2(b). To divide the slow and fast dynamics of the system, we will perform similitude transformation on the gene autoregulation model, and the central manifold describing the trajectory of slow dynamics
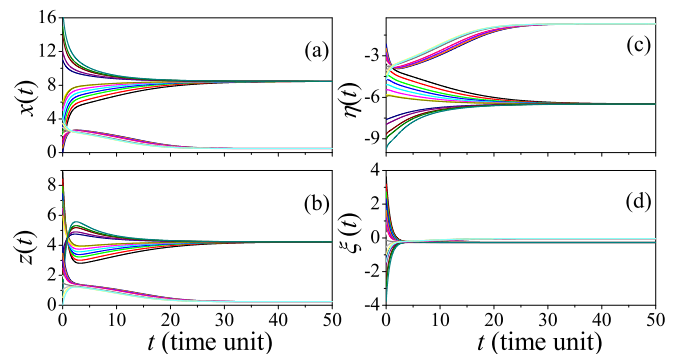

FIG. 2. Timescales are separated by transforming variables (x, z) to (η, ξ). Solutions of the system converge to the stable fixed points for different initial conditions: (a) $x(t)$, (b) $z(t)$, (c) $\eta(t)$, (d) $\xi(t)$. The system is bistable for $\gamma = 8.75$.

is obtained. Suppose that (x_s, z_s) is a stable fixed point. The right-hand sides in Eq. (1) are divided into linear and nonlinear parts, where the former is the first-order term of the Taylor series. The model can be rewritten as

$$\frac{d}{dt}\begin{pmatrix} x \\ z \end{pmatrix} = \begin{pmatrix} -\delta & \phi \\ \rho & -\tau \end{pmatrix}\begin{pmatrix} x \\ z \end{pmatrix} + \begin{pmatrix} \beta \frac{z^m}{\gamma+z^m} + \varphi - \phi z \\ 0 \end{pmatrix}, \quad (2)$$

where $\phi = \frac{\beta\gamma m z^{m-1}}{(z^m+\gamma)^2}\big|_{z=z_s}$ and $\begin{pmatrix} -\delta & \phi \\ \rho & -\tau \end{pmatrix}$ is a Jacobian matrix. The corresponding eigenvalues are as follows:

$$\lambda_{1,2} = \frac{-\delta - \tau \pm \sqrt{(\delta - \tau)^2 + 4\phi\rho}}{2}, \quad (3)$$

which define two timescales with a large difference. For example, $\lambda_2/\lambda_1 = 4.426, 9.930$ for parameter $\gamma = 8.75$, which correspond to the two stable states. To divide the two timescales, we perform a similitude transformation on Eq. (2).

$$\frac{d}{dt}\begin{pmatrix} \eta \\ \xi \end{pmatrix} = \begin{pmatrix} \lambda_1 & 0 \\ 0 & \lambda_2 \end{pmatrix}\begin{pmatrix} \eta \\ \xi \end{pmatrix} + \mathbf{T}^{-1}\begin{pmatrix} \beta \frac{z^m}{\gamma+z^m} + \varphi - \phi z \\ 0 \end{pmatrix}, \quad (4)$$

where $\begin{pmatrix} \eta \\ \xi \end{pmatrix} = \mathbf{T}^{-1}\begin{pmatrix} x \\ z \end{pmatrix}$, and the similitude transformation matrices are given by

$$\mathbf{T} = \begin{pmatrix} 2\phi & 2\phi \\ \delta - \tau + M & \delta - \tau - M \end{pmatrix},$$

$$\mathbf{T}^{-1} = \frac{1}{4\phi M}\begin{pmatrix} \delta - \tau - M & -2\phi \\ \tau - \delta - M & 2\phi \end{pmatrix}, \quad (5)$$

where $M = \sqrt{(\delta - \tau)^2 + 4\phi\rho}$. Eigenvector η is a slow variable, whereas ξ is a fast variable. Figure 2 shows the transient process of the bistable system, for which two stable fixed points are given by $(x_s, z_s) = (0.478, 0.239)$ and $(8.457, 4.229)$, or $(\eta_s, \xi_s) = (-0.691, -0.048)$ and $(-6.482, -0.275)$. The stable states are in agreement with the bifurcation diagram shown in Ref. [33]. Starting from different initial conditions, variables x and z converge to the fixed points at almost the same time scale, whereas η converges to the fixed points considerably slower than ξ. Thus, the slow and fast dynamics are separated successfully. It should be pointed out that the separation of timescales is completely different from the separation of gradient and nongradient components [2,5–10].

After a short transient process, $\dot{\xi} \approx 0$ allows us to obtain an equation, which will be denoted by $x = f(z)$ as follows:

$$x = \frac{2\beta\frac{z^m}{\gamma+z^m} + 2\varphi - 2\phi z}{\delta + \tau + M} - \frac{2\phi z}{\tau - \delta - M}. \quad (6)$$

After a short transient process, the system will converge to the manifold determined by Eq. (6), namely, central manifold, and then slowly approach one of the stable fixed points along the central manifold. The dark line in Fig. 3(a) represents the central manifold curve of the bistable autoregulation model with $\gamma = 8.75$, and the two solid circles indicate the stable states separated by one unstable fixed point (hollow circle). In Eq. (6), curve $x = f(z)$ depends on the stable fixed points (x_s, z_s). When we determine the central manifold on the basis of one of the two stable fixed points, the other will slightly deviate from the central manifold. As a compromise, we obtain the left part of the central manifold on the basis of the
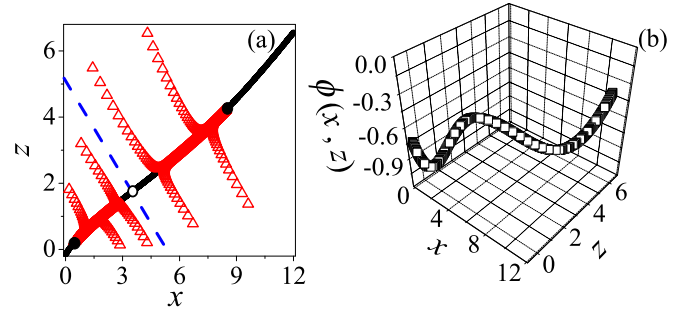

FIG. 3. (a) The central manifold of the bistable gene autoregulation model for $\gamma = 8.75$. The black thick line represents the central manifold curve, while the red triangles depict how the system converges to the steady states from different initial states. The dashed blue line separates the attraction region of the two stable states. The solid circles are the stable fixpoints, whereas the hollow circle is the unstable one. (b) The 1D potential curve along the central manifold shown in (a).

left stable fixed point, whereas the right part is calculated on the basis of the right one. The two parts are divided by the unstable fixed point. Figure 3(a) shows that all time evolutions of the system may be divided into two 1D parts: quickly converging to the central manifold and slowly approaching the stable fixed points along the central manifold.

We focus on the slow dynamics along $x = f(z)$. This dynamics is governed by the following 1D equation:

$$\dot{\eta} = \lambda_1\eta + g[z(\eta)]$$
$$= \lambda_1\eta + \frac{\delta - \tau - M}{4\phi M}\left(\beta\frac{z^m}{\gamma + z^m} + \varphi - \phi z\right). \quad (7)$$

The 1D slow dynamics allows us to obtain the 1D energy landscape along the central manifold by

$$\phi(x, z) = \phi(\eta) = -\int_{\eta_0}^{\eta}\{\lambda_1\eta' + g[z(\eta')]\}d\eta'$$
$$= -\int_{\eta_0}^{\eta}(\lambda_1\eta')d\eta' - \int_{z_0}^{z}g(z')\frac{d\eta'}{dz'}dz', \quad (8)$$

where the last part of the integration over η is transformed to z by deriving their relationship on the basis of Eq. (6) and transformation matrix $\mathbf{T}$. The derivative is given by

$$\frac{d\eta}{dz} = \frac{1}{2\phi M}\left(\frac{\delta - \tau - M}{\delta + \tau + M}\frac{\beta\gamma m z^{m-1}}{(z^m + \gamma)^2} + \phi\frac{2M}{\tau - \delta - M}\right.$$
$$\left. - \phi\frac{\delta - \tau - M}{\delta + \tau + M}\right) \quad (9)$$

Figure 3(b) shows the bistable 1D potential along the central manifold. The two valleys on the energy landscape indicate two stable fixed points, whereas the peak corresponds to an unstable one. The extrema of ϕ are in good agreement with the position of fixed points.

We should focus on the fast dynamics to extend the 1D energy landscape along the central manifold to 2D configuration space. The system quickly converges to the central manifold along the straight lines [Fig. 3(a)]. The slopes of all straight lines are approximately the same, which also equals that of the blue line in Fig. 3(a). The slopes can be estimated on the
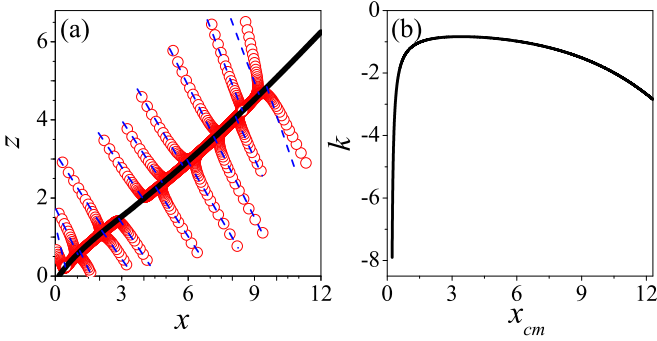
FIG. 4. (a) Red circles illustrate how the system converges to the fixed points from different initial conditions. The dashed blue lines show the theoretically obtained slopes of the straight lines; (b) theoretical estimated slopes as a function of the points in the central manifold. The model is bistable for $\gamma = 8.75$.

basis of the fast dynamics of the system. In fact, slow variable $\eta(t)$ changes slightly compared with $\xi(t)$, thus, we can obtain the slope by setting a constant value of $\eta(t)$.

$$\eta = (\delta - \tau - M)x - 2\phi z = \text{const} \tag{10}$$

and the slope is

$$k = \left.\frac{\delta - \tau - M}{2\phi}\right|_{z=z_{\text{cm}}}. \tag{11}$$

These results allow us to calculate the 1D energy landscape along the straight lines.

$$z - z_{\text{cm}} = k(x - x_{\text{cm}}) \tag{12}$$

where $(x_{\text{cm}}, z_{\text{cm}})$ corresponds to the points along the central manifold. In Fig. 4(a), the dashed blue lines indicate the slopes obtained using the theoretical method. Theoretical results are in good agreement with the time evolution of the systems (red circles). However, when the system tends to converge to states far from the unstable fixed point, the theoretically estimated values of k will deviate from the time evolutions.

By plugging Eq. (12) into Eqs. (1), we can obtain a 1D system $\dot{x} = h(x)$. The 1D system potential can be calculated
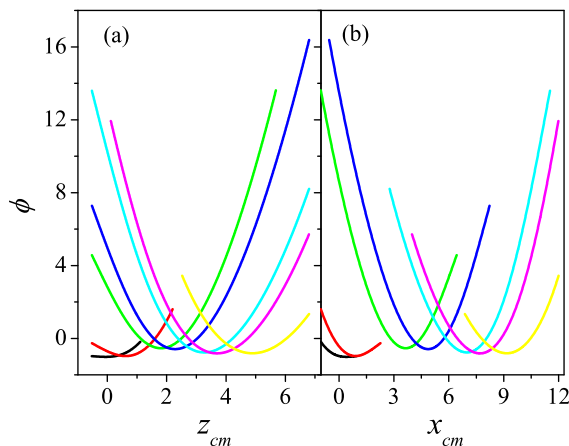

FIG. 5. 1D potential curves are calculated along the straight lines, where $\gamma = 8.75$.
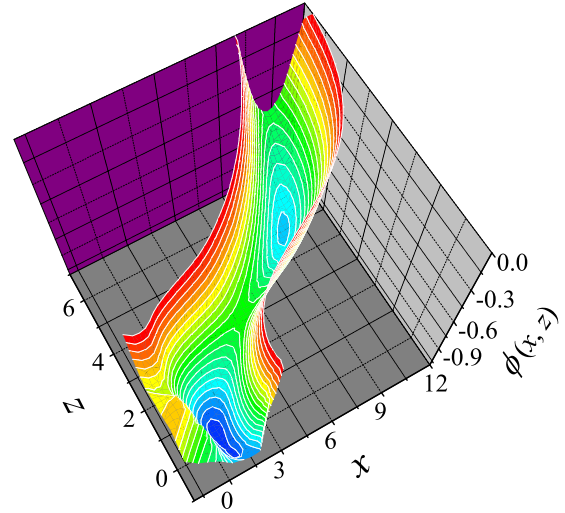

FIG. 6. 2D potential surfaces for the bistable gene autoregulation model with $\gamma = 8.75$.

as

$$\phi(x) = -\int_{x_0}^{x} h(x')dx'. \tag{13}$$

Figure 5 shows the 1D potentials calculated along the fast process [triangles in Fig. 3(a) and circles in Fig. 4(a)] for $(x_{\text{cm}}, z_{\text{cm}})$. The minimum values of the potential curves correspond to the intersection point of the straight lines and central manifold, thereby implying that the system converges to the manifold along the straight lines.

By integrating the potential along the central manifold and straight lines, we can obtain the 2D energy landscape of the system. Figure 6 shows the energy landscape of the bistable
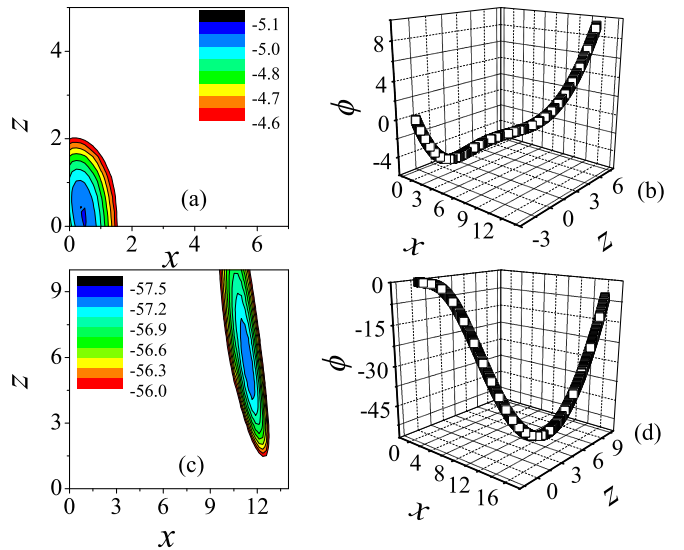

FIG. 7. Energy landscape of the monostable gene autoregulation model. 2D energy landscapes are displayed by colored contour figures in (a) $\gamma = 11.5$ and (c) $\gamma = 3$. (b) and (d) show the corresponding 1D potential along the central manifolds. The potential values of the white area in (a) and (c) are considerably larger than those represented by the colored bars.
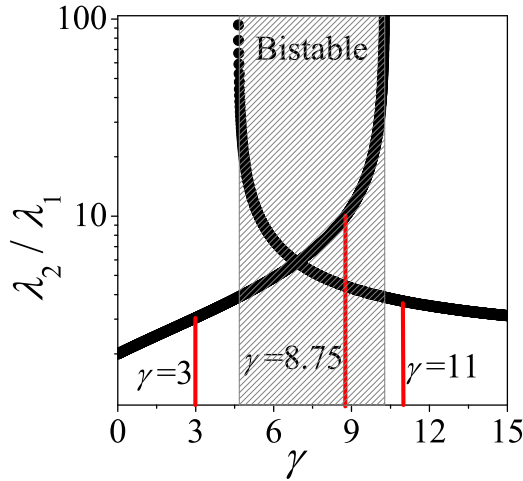
FIG. 8. The ratio of two eigenvalues λ_2/λ_1 for different values of parameter γ. The shadowed region indicates bistable area, outside which the system is monostable. The three red lines highlight the three values of γ, for which the energy landscapes are calculated in the paper.

gene autoregulation model. The valleys on the 2D surfaces represent the positions of the stable fixed points.

This theoretical method can also be used to estimate the energy landscape of the monostable system. Figure 7 represents the energy landscapes of the monostable gene autoregulation model for $\gamma = 11.5$ and 3. The model has only one fixed point $(x_s, z_s) = (0.453, 0.227)$ for $\gamma = 11.5$, and $(x_s, z_s) = (11.383, 5.691)$ for $\gamma = 3$. The minimal values of potential in Fig. 7 are in good agreement with the stable fixed points. In this paper, the energy landscapes are much steeper than that obtained through decomposing the gradient and nongradient components [2,5,6], i.e., the potential value on the central manifold is much lower than that outside it. The high steepness indicates the dynamics outside the central manifold is very fast. That illustrates the rationality for our method to separate timescales, and imply our method is only adapted for the 2D system, whose dynamics could be separated to distinct timescales.

Our method is based on a notion that the 2D dynamics can be divided into two 1D parts with separated timescales. The method is further effective when the difference between timescales is large. As shown in Eqs. (3) and (4), λ_2/λ_1 can be used to quantify the difference between timescales. The ratio is depicted as a function of the bifurcation parameter γ of the gene autoregulation model in Fig. 8. The value of λ_2/λ_1

in the bistable region is considerably larger than that in the monostable region, which may imply that the method is more effective for the bistable model than the monostable model. On the other hand, we can see that there are two values for the ratio in the bistable region, which are calculated on the basis of the two stable fixed points. One of the two values will increase dramatically when the value of γ approaches the bifurcation points. However, a large increase in ratio does not correspond to improved effectiveness because the other ratio is decreased.

IV. SUMMARY

We present an elegant and comprehensive method estimating the 2D energy landscape of a bistable gene autoregulation model. The 2D system is divided into two 1D systems theoretically working on distinct timescales, and the two 1D potentials are calculated through integration because 1D systems can always be regarded as gradient systems. Then, the 2D energy landscape is obtained by integrating the two 1D potentials. For the gene autoregulation model, the slow part represents the dynamics process along the central manifold, whereas the fast part indicates the convergence process to the central manifold along straight lines.

Our method is an approximation because the separation of fast and slow dynamics is based on an approximation: the slow variable is constant in the 1D fast system, and *vice versa*. The approximation is reasonable when the two timescales are distinct. Thus, the more distinct the fast and slow dynamics, the more effective the method. Our method is suitable for all 2D systems, the dynamics of which can be divided into fast and slow parts, regardless if the system is monostable or bistable. In fact, a nonlinear biological system with this type of characteristic is ubiquitous, such as the genetic toggle switch [10,25] and double-gene positively interlinked regulatory [11,13,21] models. We can separate the slow and fast dynamics for these models via similitude transformation. A model type is even represented by the FitzHugh-Nagumo neuron model, in which two variables in the original system are working on two distinct timescales [37].

[1] J. Wang, K. Zhang, L. Xu, and E. Wang, Quantifying the Waddington landscape and biological paths for development and differentiation, Proc. Natl. Acad. Sci. USA **108**, 8257 (2011).

[2] J. X. Zhou, M. D. S. Aliyu, E. Aurell, and S. Huang, Quasi-potential landscape in complex multi-stable systems, J. R. Soc. Interface **9**, 3539 (2012).

[3] P. Ao, Global view of bionetwork dynamics: Adaptive landscape, J. Genet. Genomics **36**, 63 (2009).

[4] L. Yin and P. Ao, Existence and construction of dynamical potential in nonequilibrium processes without detailed balance, J. Phys. A: Math. Gen. **39**, 8593 (2006).

[5] C. Lv, X. Li, F. Li, and T. Li, Constructing the energy landscape for genetic switching system driven by intrinsic noise, PLoS One **9**, e88167 (2014).

[6] X. Qiu, S. Ding, and T. Shi, From understanding the development landscape of the canonical fate-switch pair to constructing

a dynamiclandscape for two-step neural differentiation, PLoS One **7**, e49271 (2011).

[7] J. Wang, L. Xu, E. Wang, and S. Huang, The potential landscape of genetic circuits imposes the arrow of time in stem cell differentiation, Biophys. J. **99**, 29 (2010).

[8] M. A. Micheelsen, N. Mitarai, K. Sneppen, and I. B. Dodd, Theory for stability and regulation of epigenetic landscapes, Phys. Biol. **7**, 026010 (2010).

[9] J. Wang, L. Xu, and E. Wang, Potential landscape and flux framework of nonequilibrium networks: Robustness, dissipation, and coherence of biochemical oscillations, Proc. Natl. Acad. Sci. USA **105**, 12271 (2008).

[10] K. Kim and J. Wang, Potential energy landscape and robustness of a gene regulatory network: Toggle switch, PLoS Comput. Biol. **3**, e60 (2007).

[11] X. P. Zhang, Z. Cheng, F. Liu, and W. Wang, Linking fast and slow positive feedback loops creates an optimal bistable switch in cell signaling, Phys. Rev. E **76**, 031924 (2007).

[12] A. N. Pisarchik and U. Feudel, Control of multistability, Phys. Rep. **540**, 167 (2014).

[13] J. Tang, X. Yang, J. Ma, and Y. Jia, Noise effect on persistence of memory in a positive-feedback gene regulatory circuit, Phys. Rev. E **80**, 011907 (2009).

[14] W. Xiong and J. E. Ferrell, A positive-feedback-based bistable 'memory module' that governs a cell fate decision, Nature (London) **426**, 460 (2003).

[15] M. Acar, A. Becskei, and A. van Oudenaarden, Enhancement of cellular memory by reducing stochastic transitions, Nature (London) **435**, 228 (2005).

[16] M. Laurent and N. Kellershohn, Multistability: A major means of differentiation and evolution in biological systems, Trends Biochem. Sci. **24**, 418 (1999).

[17] F. R. Cross, V. Archambault, M. Miller, and M. Klovstad, Testing a mathematical model of the yeast cell cycle, Mol. Biol. Cell **13**, 52 (2003).

[18] J. R. Pomerening, E. D. Sontag, and J. E. Ferrell, Testing a mathematical model of the yeast cell cycle, Nat. Cell Biol. **5**, 346 (2003).

[19] C. P. Bagowski and J. E. Ferrell, Bistability in the JNK cascade, Curr. Biol. **11**, 1176 (2001).

[20] C. Bagowski, J. Besser, C. R. Frey, and J. E. Ferrell, The JNK cascade as a biochemical switch in mammalian cells: Ultrasensitive and all-or-none responses, Curr. Biol. **13**, 315 (2003).

[21] P. Smolen, D. A. Baxter, and J. H. Byrne, Interlinked dual-time feedback loops can enhance robustness to stochasticity and persistence of memory, Phys. Rev. E **79**, 031902 (2009).

[22] D. Angeli, J. E. Ferrell, Jr., and E. D. Sontag, Detection of multistability, bifurcations, and hysteresis in a large class of

biological positive-feedback systems, Proc. Natl. Acad. Sci. USA **101**, 1822 (2004).

[23] A. Hoffmann, A. Levchenko, M. L. Scott, and D. Baltimore, The IκB-NF-κB signaling module: Temporal control and selective gene activation, Science **298**, 1241 (2002).

[24] W. Yu, J. Tang, J. Ma, J. Luo, and X. Yang, Damped oscillations in a multiple delayed feedback NFκB signaling module, Eur. Biophys. J. **44**, 677 (2015).

[25] R. Perez-Carrasco, P. Guerrero, J. Briscoe, and K. M. Page, Intrinsic noise profoundly alters the dynamics and steady state of morphogen controlled bistable genetic switches, PLoS Comput. Biol. **12**, e1005154 (2016).

[26] Y. Saka and J. C. Smith, A mechanism for the sharp transition of morphogen gradient interpretation in *Xenopus*, BMC Dev. Biol. **7**, 47 (2007).

[27] J. Cotterell and J. Sharpe, An atlas of gene regulatory networks reveals multiple three-gene mechanisms for interpreting morphogen gradients, Mol. Syst. Biol. **6**, 425 (2010).

[28] J. L. Cherry, and F. R. Adler, How to make a biological switch, J. Theor. Biol. **203**, 117 (2000).

[29] T. R. Sokolowski, T. Erdmann, and P. R. T. Wolde, Mutual repression enhances the steepness and precision of gene expression boundaries, PLoS Comput. Biol. **8**, e1002654 (2012).

[30] J. Wang, K. Zhang, and E. Wang, Kinetic paths, time scale, and underlying landscapes: A path integral framework to study global natures of nonequilibrium systems and networks, J. Chem. Phys. **133**, 125103 (2010)

[31] R. Guantes and J. F. Poyatos, Multistable decision switches for flexible control of epigenetic differentiation, PLoS Comput. Biol. **4**, e1000235 (2008).

[32] B. Verd, A. Crombach, and J. Jaeger, Classification of transient behaviours in a time-dependent toggle switch model, BMC Syst. Biol. **8**, 43 (2014).

[33] B. M. S. Arani, M. Mahmoudi, L. Lahti, J. González, and E. C. Wit, Stability estimation of autoregulated genes under Michaelis-Menten-type kinetics, Phys. Rev. E **97**, 062407 (2018).

[34] T. Chen, H. L. He, and G. M. Church, Modeling gene expression with differential equations, Pac. Symp. Biocomput. **4**, 29 (1999).

[35] T. Äijö and H. Lähdesmäki, Learning gene regulatory networks from gene expression measurements using non-parametric molecular kinetics, Bioinformatics **25**, 2937 (2009).

[36] H. D. Jong, Modeling and smulation of genetic regulatory systems: A literature review, J. Comput. Biol. **9**, 67 (2002).

[37] A. Zaikin, J. García-Ojalvo, R. Báscones, E. Ullner, and J. Kurths, Doubly Stochastic Coherence via Noise-Induced Symmetry in Bistable Neural Models, Phys. Rev. Lett. **90**, 030601 (2003).